PHYSICAL REVIEW D **82,** 024016 (2010)

Tidal Love numbers of neutron and self-bound quark stars

Sergey Postnikov[*] and Madappa Prakash[†]
Department of Physics and Astrononmy, Ohio University, Athens, Ohio 45701-2979, USA

James M. Lattimer[‡]
Department of Physics and Astronomy, State University of New York at Stony Brook, Stony Brook, New York 11794-3800, USA
(Received 28 April 2010; published 15 July 2010)

Gravitational waves from the final stages of inspiraling binary neutron stars are expected to be one of the most important sources for ground-based gravitational wave detectors. The masses of the components are determinable from the orbital and chirp frequencies during the early part of the evolution, and large finite-size (tidal) effects are measurable toward the end of inspiral, but the gravitational wave signal is expected to be very complex at this time. Tidal effects during the early part of the evolution will form a very small correction, but during this phase the signal is relatively clean. The accumulated phase shift due to tidal corrections is characterized by a single quantity related to a star's tidal Love number. The Love number is sensitive, in particular, to the compactness parameter M/R and the star's internal structure, and its determination could provide an important constraint to the neutron star radius. We show that Love numbers of self-bound strange quark matter stars are qualitatively different from those of normal neutron stars. Observations of the tidal signature from coalescing compact binaries could therefore provide an important, and possibly unique, way to distinguish self-bound strange quark stars from normal neutron stars. Tidal signatures from self-bound strange quark stars with masses smaller than $1M_\odot$ are substantially smaller than those of normal stars owing to their smaller radii. Thus tidal signatures of stars less massive than $1M_\odot$ are probably not detectable with Advanced LIGO. For stars with masses in the range 1–$2M_\odot$, the anticipated efficiency of the proposed Einstein telescope would be required for the detection of tidal signatures.

DOI: 10.1103/PhysRevD.82.024016 PACS numbers: 04.40.Dg, 26.60.Kp, 95.85.Sz, 97.60.Jd

I. INTRODUCTION

Gravitational waves from the final stages of inspiraling binary neutron stars are expected to be one of the most important sources for ground-based gravitational wave detectors [1]. To date, LIGO observations have only been able to set an upper limit to the neutron star-neutron star coalescence rate of 0.039 $\mathrm{yr}^{-1}L_{10}^{-1}$ [2], where L_{10} is the blue luminosity in units of $10^{10}L_\odot$, which translates to about 0.075 events per year in the Milky Way. This is a thousand times larger than the predicted rates [3]. Nevertheless, the observed neutron star-neutron star inspiral rate from the universe is expected to be about two per day in LIGO II [3]. The masses of the components will be determined to moderate accuracy, especially if the neutron stars are slowly spinning, during the early part of the evolution [4,5].

Mass measurements from inspiraling binaries will be useful, especially in constraining the equation of state through limits to the neutron star maximum and minimum masses, but constraints to the radius would be much more effective in constraining the nuclear equation of state [6]. Large finite-size effects, such as mass exchange and tidal disruption, are measurable toward the end of inspiral [7], but the gravitational wave signal is expected to be very complex during this period. Flanagan and Hinderer [8] have recently pointed out that tidal effects are also potentially measurable during the early part of the evolution when the waveform is relatively clean. The tidal fields induce quadrupole moments on the neutron stars. This response of each star to external disturbance is described by the Love number k_2 [9], which is a dimensionless coefficient given by the ratio of the induced quadrupole moment Q_{ij} and the applied tidal field E_{ij}:

$$Q_{ij} = -k_2 \frac{2R^5}{3G} E_{ij} \equiv -\lambda E_{ij}, \tag{1}$$

where R is the radius of the star and G is the gravitational constant. The tidal Love number k_2, which is dimensionless, depends on the structure of the star and therefore on the mass and the equation of state (EOS) of dense matter. The quantity λ is the induced quadrupole polarizability.

Tidal effects will form a very small correction in which the accumulated phase shift can be characterized by a single quantity $\bar{\lambda}$ which is a weighted average of the induced quadrupole polarizabilities for the individual stars, λ_1 and λ_2. Since both neutron stars have the same equation of state, the weighted average $\bar{\lambda}(\mathcal{M})$, as a function of chirp

[*]sp315503@ohio.edu
[†]prakash@harsha.phy.ohiou.edu
[‡]lattimer@astro.sunysb.edu

mass $\mathcal{M} = m_1^{3/5} m_2^{3/5}/(m_1 + m_2)^{1/5}$, is relatively insensitive to the mass ratio m_1/m_2, as is shown by Hinderer *et al.* [10]. We therefore focus on the behavior of the quadrupole polarizability λ of individual stars. These are related to the dimensionless tidal Love number k_2 for each star by $k_2 = (3/2)G\lambda R^{-5}$. The Love number k_2 is sensitive to the neutron star equation of state; in particular, to the compactness parameter M/R as shown by Damour and Nagar [11] and the overall compressibility of the equation of state. In particular, the tidal Love numbers of strange quark matter stars are qualitatively different from those of normal matter stars. In a fashion similar to moment of inertia measurements from relativistic binary pulsars [12], an important constraint to the neutron star radius might become possible from gravitational wave observations. Detection of the tidal signature from coalescing compact binaries might provide an important, and possibly unique, way to distinguish self-bound strange quark matter stars from normal neutron stars.

Our paper is organized as follows. In Sec. I, a new technique for the computation of tidal Love numbers is described. The influence of density discontinuities and phase transitions on Love numbers is discussed in Sec. II. Results of Love numbers for polytropic equations of state are presented in Sec. IV. Section V contains results for select analytic solutions of Einstein's equations in spherical symmetry. Love numbers for proposed model equations of state for normal stars with hadronic matter and self-bound stars with strange quark matter with and without crusts are given in Sec. VI, wherein a comparison of results between these two distinct classes of stars is also made. In Sec. VII, we discuss the role of a solid crust on Love numbers. Our results and conclusions are summarized in Sec. VIII. Appendix A contains technical details concerning the calculation of Love numbers in the case of polytropes. Relevant parameters required for the computation of Love numbers for analytic solutions of Einstein's equations (discussed in Sec. V) are to be found in Appendix B.

II. COMPUTATION OF TIDAL LOVE NUMBERS

The computation of tidal Love numbers is described by Thorne and Campolattaro [13], Hinderer [14], Damour and Nagar [11]. We use units in which $G = c = 1$. In terms of the dimensionless compactness parameter $\beta = M/R$, the Love number is given by

$$\begin{aligned} k_2(\beta, y_R) = {} & \tfrac{8}{5}\beta^5(1-2\beta)^2[2 - y_R + 2\beta(y_R - 1)] \\ & \times \{2\beta(6 - 3y_R + 3\beta(5y_R - 8) \\ & + 2\beta^2[13 - 11y_R + \beta(3y_R - 2) \\ & + 2\beta^2(1 + y_R)]) + 3(1-2\beta)^2[2 - y_R \\ & + 2\beta(y_R - 1)\}\log(1-2\beta)]^{-1}. \end{aligned} \tag{2}$$

Here, $y_R = [rH'(r)/H(r)]_{r=R}$, where the function $H(r)$ is the solution of the differential equation

$$\begin{aligned} H''(r) + H'(r)\left[\frac{2}{r} + e^{\lambda(r)}\left(\frac{2m(r)}{r^2} + 4\pi r(p(r) - \rho(r))\right)\right] \\ + H(r)Q(r) = 0, \end{aligned} \tag{3}$$

where the primes denote derivatives with respect to r, and

$$\begin{aligned} Q(r) = {} & 4\pi e^{\lambda(r)}\left(5\rho(r) + 9p(r) + \frac{\rho(r) + p(r)}{c_s^2(r)}\right) \\ & - 6\frac{e^{\lambda(r)}}{r^2} - (\nu'(r))^2. \end{aligned} \tag{4}$$

The metric functions $\lambda(r)$ and $\nu(r)$ for the spherical star are

$$\begin{aligned} e^{\lambda(r)} &= \left[1 - \frac{2m(r)}{r}\right]^{-1}, \\ \nu'(r) &= 2e^{\lambda(r)}\frac{m(r) + 4\pi p(r) r^3}{r^2}, \end{aligned} \tag{5}$$

and $c_s^2(r) \equiv dp/d\rho$ is the squared sound speed. Care has to be taken in the event of a first-order phase transition or a surface density discontinuity in the evaluation of Eq. (3) because the speed of sound vanishes. We address this situation in the next section.

We note that the calculation of the tidal Love number is simplified by casting Eq. (3) as a first-order differential equation for $y(r) = rH'(r)/H(r)$:

$$\begin{aligned} ry'(r) + y(r)^2 + y(r)e^{\lambda(r)}[1 + 4\pi r^2(p(r) - \rho(r))] \\ + r^2 Q(r) = 0, \end{aligned} \tag{6}$$

so that it is necessary only to determine $y_R \equiv y(R)$; the value of $H(R)$ is irrelevant. The boundary condition for Eq. (6) is $y(0) = 2$.

Damour and Nagar [11] have emphasized that the factor $(1 - 2\beta)^2$ multiplying Eq. (2) makes k_2 decrease rapidly with compactness β. Additionally, we note that for small compactness parameter β, there are severe cancellations in Eq. (2), and it is useful to expand it in a Taylor series for $\beta < 0.1$:

$$k_2(\beta, y_R) = \frac{(1-2\beta)^2}{2}\Big[\frac{2-y_R}{3+y_R} + \frac{y_R^2 - 6y_R - 6}{(y_R+3)^2}\beta + \frac{y_R^3 + 34y_R^2 - 8y_R + 12}{7(y_R+3)^3}\beta^2 + \frac{y_R^4 + 62y_R^3 + 84y_R^2 + 48y_R + 36}{7(y_R+3)^4}\beta^4 + \frac{5}{294}\frac{5y_R^5 + 490y_R^4 + 1272y_R^3 + 1884y_R^2 + 1476y_R + 648}{(y_R+3)^5}\beta^5 + \cdots\Big]. \quad (7)$$

Note that in the Newtonian limit, $\beta \to 0$, we have $p \ll \rho$, $\rho r^2 \ll 1$, and one finds

$$ry'(r) + y(r)^2 + y(r) - 6 + 4\pi r^2 \frac{\rho(r)}{c_s^2(r)} = 0, \qquad k_2(y_R) = \frac{1}{2}\left(\frac{2-y_R}{3+y_R}\right). \quad (8)$$

Equation (6) for y must be integrated with the relativistic stellar structure, or Tolman-Oppenheimer-Volkov (TOV), equations [15,16]:

$$\frac{dp(r)}{dr} = -\frac{[m(r) + 4\pi r^3 p(r)][\rho(r) + p(r)]}{r(r - 2m(r))}, \qquad \frac{dm(r)}{dr} = 4\pi\rho(r)r^2. \quad (9)$$

We find it convenient to employ a thermodynamic variable $h(r)$, defined by

$$dh(r) = \frac{dp(r)}{\rho(r) + p(r)}, \quad (10)$$

as the independent variable in place of r. A stellar model can be computed specifying the value of $h(0)$ at the star's center and integrating equations for dr/dh and dm/dh. However, since these equations are divergent at the origin and at the stellar surface, we employed the radial variable $z = r^2$ instead. One therefore has

$$\frac{dz}{dh} = -2\frac{z(\sqrt{z} - 2m)}{m + 4\pi p z^{3/2}}, \qquad \frac{dm}{dh} = 2\pi\rho\sqrt{z}\frac{dz}{dh},$$
$$\frac{dy}{dh}\nu'(h)\sqrt{z(h)}/2 = y^2 + ye^{\lambda(h)}(1 + 4\pi z(h)(p(h) - \rho(h))) + z(h)Q(h), \quad (11)$$

where Q is determined by Eq. (4). The behavior of y near the star's center is given by

$$y(h) = 2 - \frac{6}{7}\frac{5\rho_c + 9p_c + (p_c + \rho_c)/c_{sc}^2}{3p_c + \rho_c}(h_c - h) + O((h_c - h)^2). \quad (12)$$

Also note that $y_R \equiv y(h = 0)$.

In some cases, such as with polytropic equations of state, we found it was better to use $\log h$ as the independent variable. In addition, some care has to be taken in the event that $d\rho/dh$ diverges at the stellar surface, which is the case for polytropes if the polytropic index $n < 1$. In this case, the integration over the last zone near the surface can be performed analytically, as we discuss in Appendix A.

III. THE ROLE OF DENSITY DISCONTINUITIES AND PHASE TRANSITIONS

As Eq. (6) for y contains the squared adiabatic speed of sound $c_s^2 = dp/d\rho$, the solution will be altered in the case of phase transitions within the star, for example, between the crust and the core, or in the case of a finite surface density such as appears in models of strange quark stars or for a uniform density stellar model. However, in the event that multiple charges (e.g., electric charge and baryon number) are conserved in a phase transition, the constraint of global charge neutrality (two Gibb's phase rules) results in a continuous pressure versus energy density curve even if the phase transition is of first order. The situation of a density discontinuity was discussed in Damour and Nagar [11], who showed that a large discontinuity in the energy density will greatly change the value of k_2.

Expressing the sound speed in the vicinity of a density discontinuity as

$$\frac{d\rho}{dp} = \frac{1}{c_s^2} = \frac{d\rho}{dp}\Big|_{p \neq p_d} + \Delta\rho\,\delta(p - p_d), \quad (13)$$

where p_d is the pressure at the discontinuity and $\Delta\rho = \rho(p_d + 0) - \rho(p_d - 0)$ is the energy density jump across the discontinuity. While solving Eqs. (11), this discontinuity can be taken into account by properly matching solutions at the point of discontinuity $r_d = r(h_d)$:

$$y(r_d + \epsilon) = y(r_d - \epsilon) - \frac{\rho(r_d + \epsilon) - \rho(r_d - \epsilon)}{m(r_d)/(4\pi r_d^3)} = y(h_d - \epsilon) - 3\frac{\Delta\rho}{\tilde{\rho}}, \quad (14)$$

where $\epsilon \to 0$ and $\tilde{\rho} = m(r_d)/(4\pi r_d^3/3)$ is the average energy density of the inner ($r < r_d$) core.

IV. POLYTROPIC EQUATIONS OF STATE

It is useful to evaluate tidal Love numbers for polytropic equations of state $p = K\rho^{1+1/n}$. Love numbers in the Newtonian limit for polytropes have been calculated by Brooker and Olle [17] and Kokkotas and Schaefer [18]. In the Newtonian limit, it is easily observed that the values for y and k_2 are independent of the polytropic constant $K = p/\rho^{1+1/n}$, which scales out of Eq. (8). However, the quadrupole polarizability $\lambda = (2/3)k_2R^5$, and therefore the gravitational wave signature, does depend on K. There

exist analytic solutions for the Newtonian case for polytropes of indices $n = 0$ and 1. In the case $n = 0$, an incompressible fluid, $c_s^2 = \infty$ and the solution inside the star which satisfies the boundary condition at the center is simply $y(r) = 2$. However, the discontinuity in the sound speed at the stellar surface must be taken into account. According to Eq. (14), y_R receives a boundary contribution $4\pi R^3\rho/M = 3$, where ρ is the constant energy density inside the star. Therefore, for an incompressible fluid, $y_R = y(r_-) - 3 = -1$ and $k_2 = 3/4$.

In the case $n = 1$, one finds [14]

$$y(r) = \frac{\pi r}{R}\frac{J_{3/2}(\pi r/R)}{J_{5/2}(\pi r/R)} - 3, \qquad y_R = \frac{\pi^2 - 9}{3}, \qquad k_2 = \frac{15 - \pi^2}{2\pi^2}, \qquad n = 1. \tag{15}$$

In the above, $J_i(x)$ is the standard Bessel function.

Damour and Nagar [11], Hinderer [14], and Binnington and Poisson [19] have examined relativistic polytropic equations of state in the case of finite compactness. We have repeated these calculations. For each n, the polytropic constant K was determined from the fiducial pressure $p_0 = 1.322 \times 10^{-6}$ km^{-2} and $\rho_0 = 1.249 \times 10^{-4}$ km^{-2} using $K = p_o\rho_0^{-1-1/n}$. These values are equivalent to the pressure $p_0 = 1$ MeV fm^{-3} and mass-energy density $\rho_0 = 94.38$ MeV fm^{-3} (or a baryon density $n_0 = 0.1$ fm^{-3} for the case $n = 1$). These values were chosen to produce reasonable neutron star radii for solar mass neutron stars. For soft EOSs, $n > 1$, the stellar radius decreases with increasing mass up to the maximum mass and the maximum mass stars are relatively lighter than for stiff EOSs, $n < 1$. For $n < 1$, the stellar radius generally increases with increasing mass until the maximum mass is approached.

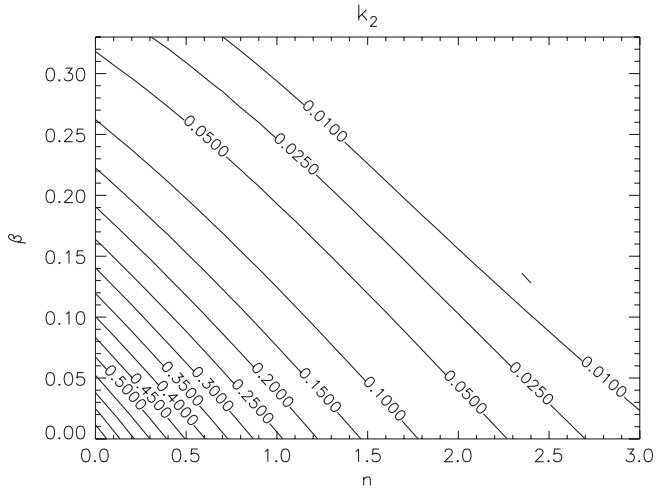

FIG. 1. Contours of the dimensionless tidal Love number k_2 as a function of compactness $\beta = M/R$ and polytropic index n (labeled along curves) for polytropes. Contours are not shown for configurations that are hydrostatically unstable (i.e., those with central densities larger than that of the maximum mass).

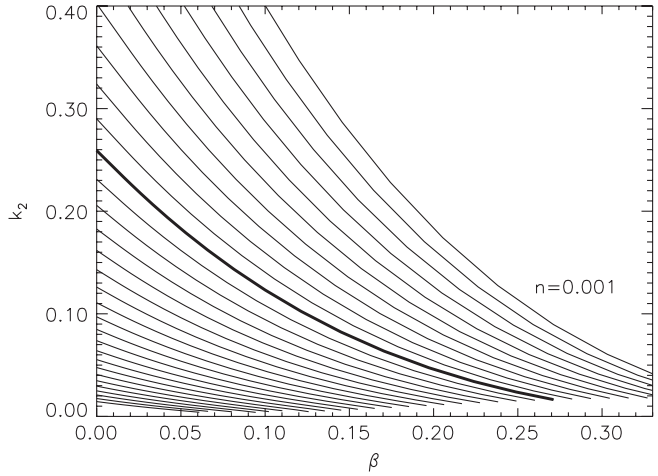

FIG. 2. The dimensionless tidal Love number k_2 as a function of compactness $\beta = M/R$ and polytropic index n for polytropes. The polytropic index $n = 0.001$ for the topmost curve and in multiples of 0.1 for each succeeding curve. The thickest curve shows results for $n = 1$.

The case $n = 1$ is intermediate and has a finite radius even for a star with vanishing mass.

The results of integrating Eq. (6) for these polytropic EOSs are summarized in Figs. 1 and 2 which show k_2 as a function of β and n. Generally, k_2 decreases with increasing n and β. The gravitational response is proportional to $\lambda = (2G/3)k_2R^5$ and this is shown for relativistic polytropes in Figs. 3 and 4. This quantity decreases rapidly with increasing n, and for $n \geq 0.5$, it also decreases rapidly with the compactness parameter β.

We have found that the results for k_2 do not significantly depend on the value K in the relativistic case by altering our fiducial values of p_o or ρ_o within reasonable ranges resulting in configurations of similar dimensions to neutron

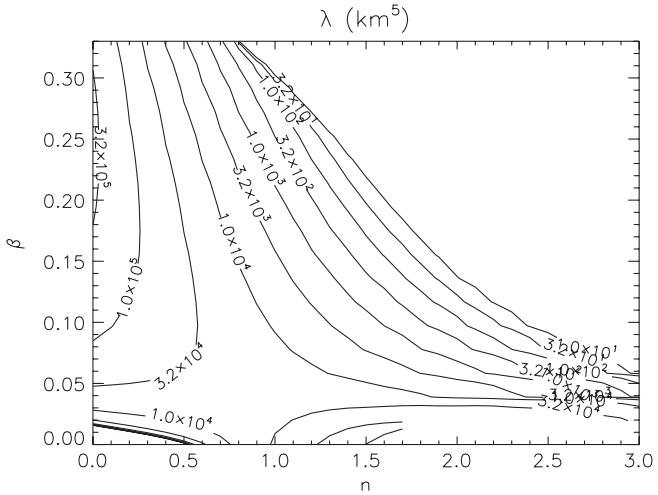

FIG. 3. The quantity $\lambda = (2G/3)k_2R^5$, in units of km^5, as a function of compactness $\beta = M/R$ for polytropes of index n. Contours are not shown for configurations that are hydrostatically unstable.

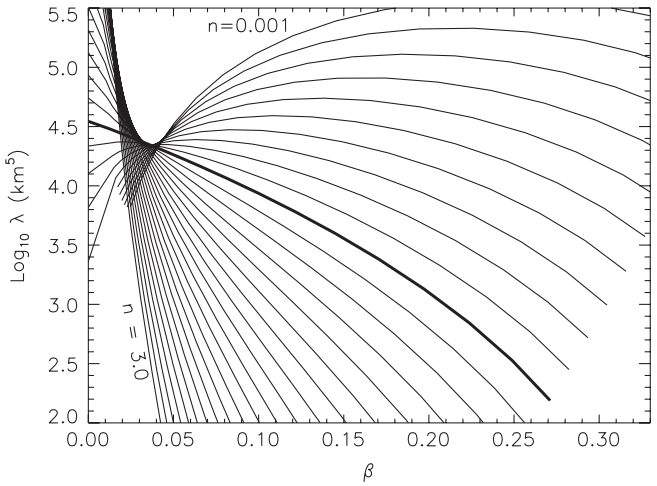

FIG. 4. The quantity $\lambda = (2G/3)k_2R^5$, in units of km^5, as a function of compactness $\beta = M/R$ for polytropes ranging from $n = 0.001$ (topmost curve) to 3.0 (leftmost curve) in increments of 0.1. Results for the polytrope $n = 1$ are shown as a thick curve.

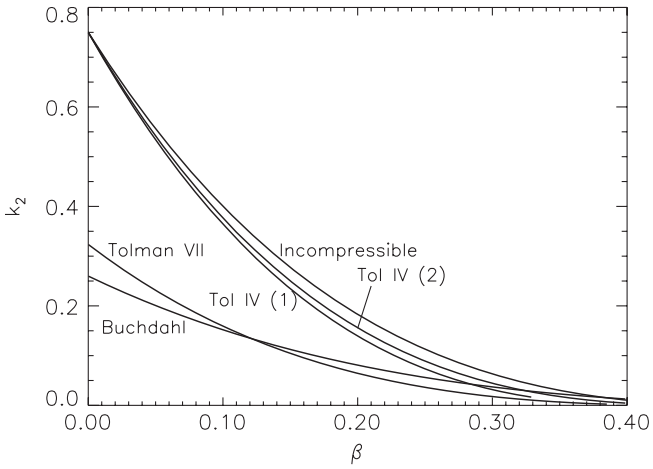

FIG. 5. The dimensionless tidal Love number k_2 as a function of compactness $\beta = M/R$ for analytic solutions (see Appendix B) of Einstein's equations in spherical symmetry.

stars. Our results are the same as those of Damour and Nagar [11], Hinderer [14], and Binnington and Poisson [19] to within numerical accuracy.

V. LOVE NUMBERS FOR ANALYTIC SOLUTIONS OF EINSTEIN'S EQUATIONS

It is also useful to compute the tidal response for some of the known analytic solutions of Einstein's equations in spherical symmetry. All analytical solutions are scale free; they contain essentially two parameters, the central energy density ρ_c and compactness parameter $\beta = GM/Rc^2$. Among the useful analytic solutions we will study are (i) the uniform fluid sphere, (ii) the Tolman VII solution [15], (iii) Buchdahl's solution [20,21], and (iv) and (v), two generalizations of the Tolman IV solution [22,23]. The Tolman VII and Buchdahl's solutions have vanishing surface energy densities and are useful approximations to realistic neutron star models. The incompressible fluid and the generalizations of the Tolman IV solution have finite surface densities, and the latter are reasonable approximations of strange quark matter stars.

It is useful to recast Eq. (11) in the form

$$\frac{dw}{dh} = -2\frac{w(\sqrt{w} - 2x\beta)}{x\beta + \alpha(p/\rho_c)w^{3/2}},$$
$$\frac{dx}{dh} = \frac{dw}{dh}\left[\frac{\alpha}{2\beta}\frac{\rho}{\rho_c}\sqrt{w}\right],$$
$$\frac{dy}{dh} = \frac{dw}{dh}\left\{-\frac{y^2 + ye^{\lambda} - 6e^{\lambda}}{2w} + \frac{\alpha}{2}e^{\lambda}\left[\left(\frac{\rho}{\rho_c} - \frac{p}{\rho_c}\right)y - 5\frac{\rho}{\rho_c} - 9\frac{p}{\rho_c} - \frac{\rho + p}{\rho_c c_s^2}\right] + \frac{2}{w}e^{2\lambda}\left(\frac{1 - e^{-\lambda}}{2} + \alpha w\frac{p}{\rho_c}\right)^2\right\}, \quad (16)$$

where $\alpha = 4\pi\rho_c R^2$, $x = m/M$, $\beta = M/R$, and $w = r^2/R^2$. Therefore, we need the quantities ρ/ρ_c, p/ρ_c, c_s^2, α, and e^{λ} for each analytic equation of state. In addition, for the Tolman IV solutions, which have a finite surface density, the boundary contribution to y_R is required. This quantity, in the present notation, is $-(\alpha/\beta)(\rho_s/\rho_c)$. The quantity ρ_s/ρ_c together with the above quantities are provided in Appendix B.

As shown in Fig. 5, the two analytic solutions that most closely resemble normal neutron stars, the Buchdahl and Tolman VII solutions, predict values of k_2 that are similar and which closely track the results for the $n = 1$ polytrope (of course, for $\beta = 0$, Buchdahl's solution and the $n = 1$ polytrope are identical). In contrast, the incompressible and Tolman IV solutions represent a significantly different family, and, as we will see, are good approximations to strange quark matter stars. It is clear that the two families of analytic solutions have different behaviors, and this foreshadows the results for the equation of state models we discuss below. Because of the scale-free character of these solutions, we have not shown results for λ, which will scale with the assumed ρ_c (or, equivalently, M or R.)

VI. LOVE NUMBERS FOR MODEL EQUATIONS OF STATE

A. Hadronic equations of state

The hadronic EOSs were taken from a compilation by Lattimer and Prakash [6] that describes their origins. There are three generic families of equations of state: (i) normal nucleonic equations of state, (ii) equations of state with considerable softening above the nuclear saturation density, due to Bose condensation, hyperons, or a mixed quark-hadronic phase, and (iii) strange quark matter stars. We have used a selection in an attempt to span the extreme range of models of each type. The mass-radius curves for hadronic EOSs are shown in Fig. 6.

TABLE I. Approach refers to the underlying theoretical technique. Composition (Comp.) refers to strongly interacting components (n = neutron, p = proton, Z = nucleus, H = hyperon, K = kaon, Q = quark); all models include leptonic contributions. This Table is slightly expanded from the version found in Ref. [32] which contains references not noted here.

Equations of state Symbol	Reference	Approach	Comp.
FP	Friedman and Pandharipande	Variational	np
WFF(1–3)	Wiringa, Fiks, and Fabrocine	Variational	np
AP(1–4)	Akmal and Pandharipande	Variational	np
MS(0–3)	Müller and Serot	Field theoretical	np
MPA(1–2)	Muther, Prakash, and Ainsworth	Dirac-Brueckner HF	np
ENG	Engvik *et al.*	Dirac-Brueckner HF	np
PAL(1–6)	Prakash, Ainsworth, and Lattimer	Schematic potential	np
GM(1–3)	Glendenning and Moszkowski	Field theoretical	npH
GS(1–2)	Glendenning and Schaffner-Bielich	Field theoretical	npK
PCL(1–2)	Prakash, Cooke, and Lattimer [33]	Field theoretical	npHQ
SLY4	Douchin and Haensel [34]	Field theoretical	npe
SQM(1–3)	Prakash, Cooke, and Lattimer [33]	Quark matter	Q (u, d, s)
STE	Jaikumar, Reddy, and Steiner [24]	Quark matter	Q (u, d, s)
PAG	Page [25]	Quark matter	Q (u, d, s)
ALF	Alford [26]	Quark matter	Q (u, d, s)
HS	Haensel, Salgado, and Bonazzola [35]	Crust	Z, e, n
BPS	Baym, Pethick, and Sutherland [36]	Crust	Z, e, n

Love numbers as a function of compactness are shown in Fig. 7 for hadronic models. There is a relatively narrow spread of values of k_2 for a given compactness, and for each EOS, the value of k_2 appears to be a maximum for masses near $1M_\odot$. In contrast to the analytic Tolman VII and Buchdahl solutions, for which $k_2(\beta \to 0) \simeq 0.3$, k_2 tends to zero for small β for realistic equations of state. The fact that hadronic equations of state have a small range of variations as a function of compactness is reminiscent of the situation for the moment of inertia [12].

It is useful to examine k_2 as a function of neutron star radius, as shown in Fig. 8. Although the range of values observed for k_2 are common to all models, it is now clear that the quadrupole response will vary more widely, due to it being proportional to R^5. In Figs. 9 and 10 the quadrupole response is shown. The maxima in λ occur near $1M_\odot$, as they did for k_2, and there is a pronounced trend for λ to increase with R. Assuming the true neutron star equation of state is hadronic, it therefore appears that a measurement of λ translates into an estimate of R relatively independently

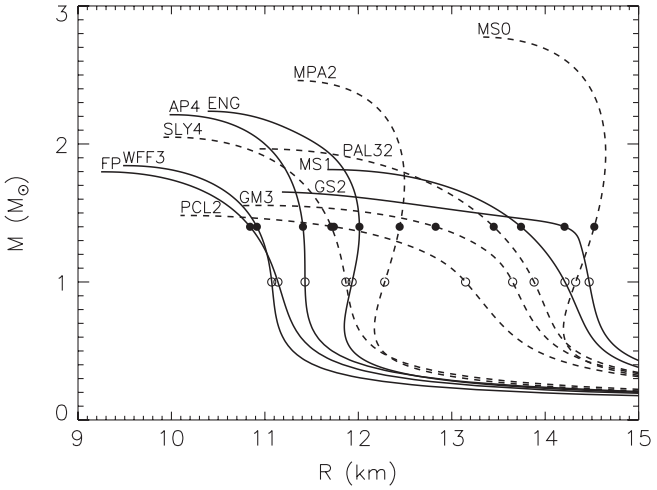

FIG. 6. Mass-radius diagram for the hadronic equations of state used in this paper. Filled (open) circles indicate configurations with $M = 1.4M_\odot$ ($1.0M_\odot$). The EOS notation follows Lattimer and Prakash [6] and Table I. The solid and dashed curves are only intended for visual clarity.

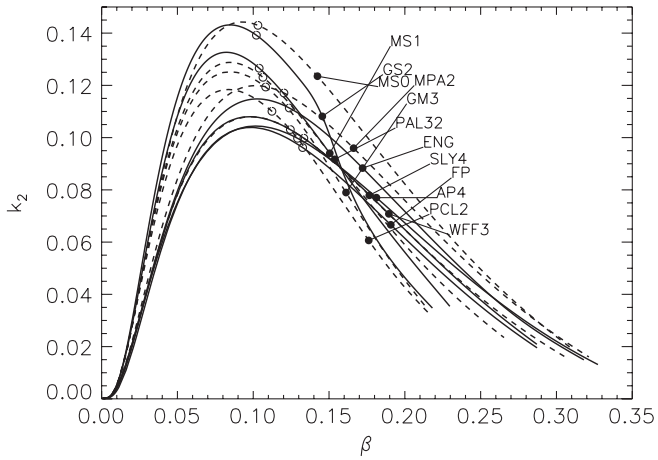

FIG. 7. The dimensionless tidal Love number k_2 as a function of compactness $\beta = M/R$ for hadronic EOSs. Filled (open) circles indicate configurations with $M = 1.4M_\odot$ ($1.0M_\odot$). The EOS notation follows Lattimer and Prakash [6] and Table I. The solid and dashed curves are only intended for visual clarity.

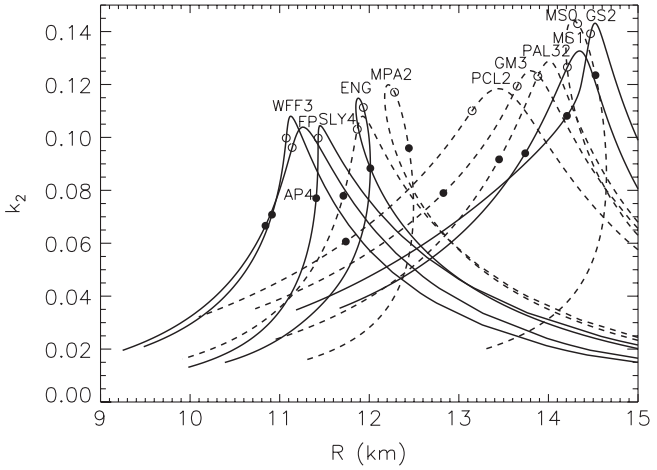

FIG. 8. The Love number k_2 as a function of radius R. Filled (open) circles indicate configurations with $M = 1.4M_\odot$ ($1.0M_\odot$). The EOS notation follows Lattimer and Prakash [6] and Table I. The solid and dashed curves are only intended for visual clarity.

of the details of the equation of state. In fact, compared to the moment of inertia which scales as R^2, the potential for a radius constraint is enhanced due to the R^5 behavior of λ.

B. Self-bound strange quark matter stars

We turn now to examine results of Love numbers for self-bound strange quark matter stars. It is uncertain whether or not strange quark matter stars will have significant crusts or not, so we examine models of both kinds. Models without crusts are characterized by quark matter extending up to a bare surface with a finite baryon density of 2 to 3 times nuclear matter equilibrium density. Crusts of normal matter on top of such stars might be supported by strong electric fields at the surface. Figure 11 shows three examples for both cases (STE from Ref. [24], PAG from Ref. [25], and ALF from Ref. [26]). The crust and the core regions are apparent from the large discontinuity in the energy density. The existence of a crust results in large radii for small stellar masses (of order $0.01M_\odot$), but do not dramatically affect the radii of stars with masses larger than $0.1M_\odot$ (see Fig. 12). It therefore appears unlikely that the existence of a crust has a pronounced effect on the Love number or quadrupole properties of the star.

In Fig. 13, the dimensionless Love number k_2 is shown as a function of compactness. As was the case for hadronic stars, there is a clustering of curves relatively independent of the EOS for stars without crusts. The curves follow the analytic results for the incompressible fluid and for the Tolman IV solutions, and differ from hadronic cases by having a large, finite value of k_2 for small β. However, in the case of an added crust, k_2 is reduced at small values of M/R, but this only occurs for ultralow mass stars. For masses in excess of $1M_\odot$, the Love number approaches the corresponding values for hadronic stars, and the effect of the crust is negligible.

The quadrupole response $\lambda = 2k_2R^5/3$ is shown in Fig. 14 as a function of radius. The strong dependence on radius follows the trend noted for hadronic stars. The effect of the crust is unimportant.

C. Comparison of normal and self-bound stars

In order to elaborate the distinction between strange quark matter and hadronic models, we show the quadrupole response $\lambda = 2k_2R^5/3$ in Fig. 15 for a representative sample of models of each type. The strong dependence of λ on R is common to all models. Where the radii of models overlap, however, it appears that the strange quark matter configurations have values of λ about 50% larger. This

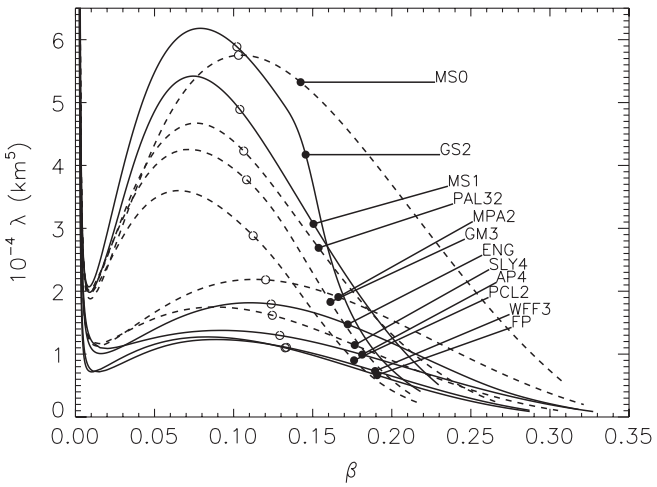

FIG. 9. The quantity $\lambda = (2/3)k_2R^5$ for hadronic equations of state. Filled (open) circles indicate configurations with $M = 1.4M_\odot$ ($1.0M_\odot$). The solid and dashed curves are only intended for visual clarity.

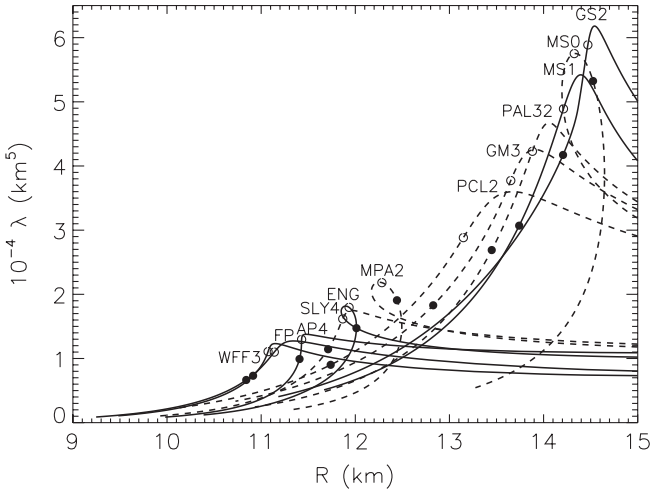

FIG. 10. The quantity $\lambda = (2/3)k_2R^5$ for hadronic equations of state. Filled (open) circles indicate configurations with $M = 1.4M_\odot$ ($1.0M_\odot$). The solid and dashed curves are only intended for visual clarity.

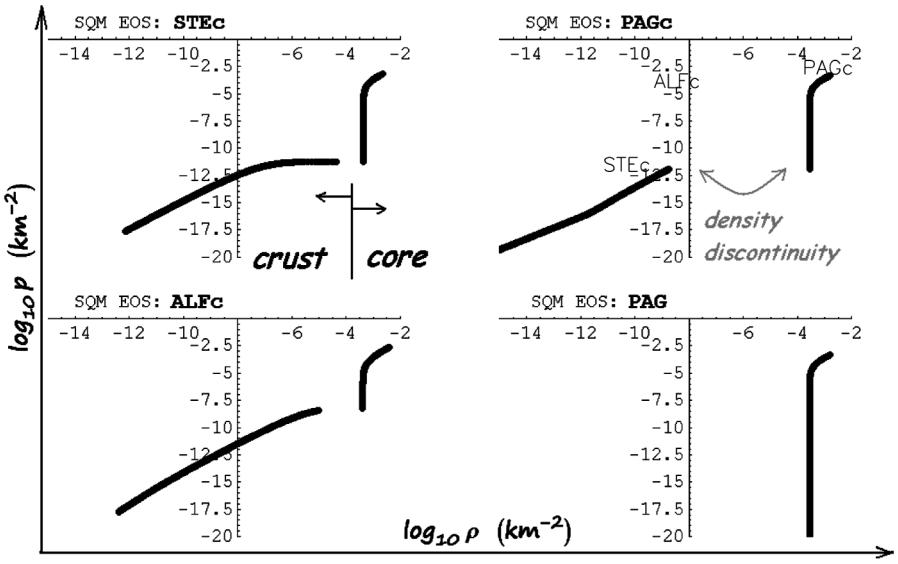

FIG. 11. Pressure versus energy density for strange quark matter equations of state with and without crust. Equation of state STE is taken from Ref. [24], PAG from Ref. [25], and ALF from Ref. [26] (see Table I). Density discontinuities are as indicated.

difference is probably too small to be observable, and it appears doubtful that any quark matter configurations will have a strong enough tidal signature to be observed.

VII. DISCUSSION

The combined tidal effects of two neutron stars in circular orbit can be found from a weighted average of the quadrupole responses [8]:

$$\tilde{\lambda} = \frac{1}{26}\left[(11m_2 + M)\frac{\lambda_1}{m_1} + (11m_1 + M)\frac{\lambda_2}{m_2}\right], \quad (17)$$

where $M = m_1 + m_2$ is the total mass of the binary and λ_1 and λ_2 are the quadrupole responses of m_1 and m_2. Note that if $m_1 = m_2$, then $\lambda_1 = \lambda_2 = \tilde{\lambda}$. If $m_2 = 0.5m_1$, then $\tilde{\lambda} \approx (40/26)\lambda_1$. It is unlikely that the mass ratio would be smaller than this amount, as the minimum neutron star mass that can be formed in supernovae is not less than $1M_\odot$ and the maximum neutron star mass is of order $2M_\odot$. Therefore, the value of $\bar{\lambda}$ is similar to that of the largest neutron star. In the case that the individual masses can be found to reasonable accuracy from the gravitational wave signal, the individual values of λ for the two stars will be determined to an accuracy constrained by the errors in $\bar{\lambda}$ and the masses.

We have assumed in evaluating the Love numbers that the crust behaves as a liquid. However, if the stress on the

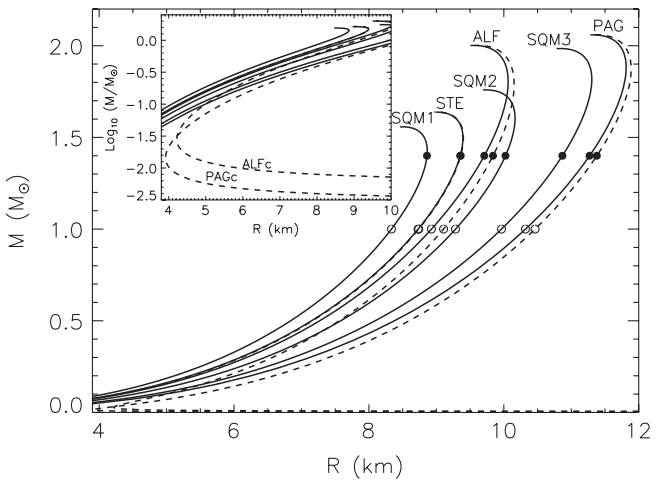

FIG. 12. Mass-radius curves for strange quark matter equations of state. The inset shows results on a logarithmic scale to highlight the effects of a hadronic crust. The solid and dashed curves are only intended for visual clarity.

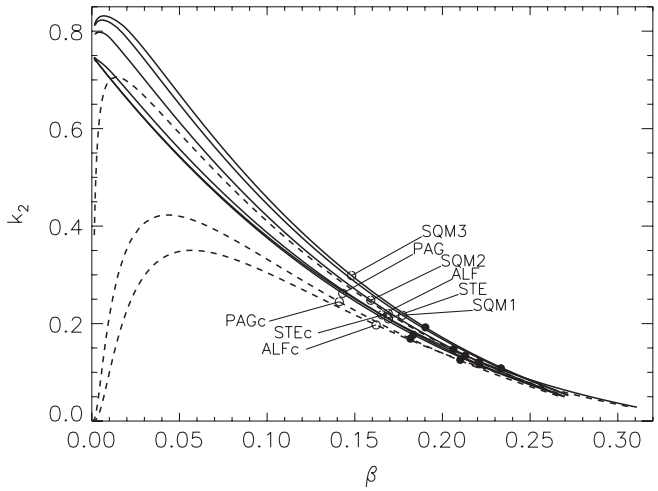

FIG. 13. Dimensionless Love numbers for the strange quark matter stars. Filled (open) circles indicate configurations with $M = 1.4M_\odot$ ($1.0M_\odot$). The solid and dashed curves are only intended for visual clarity.

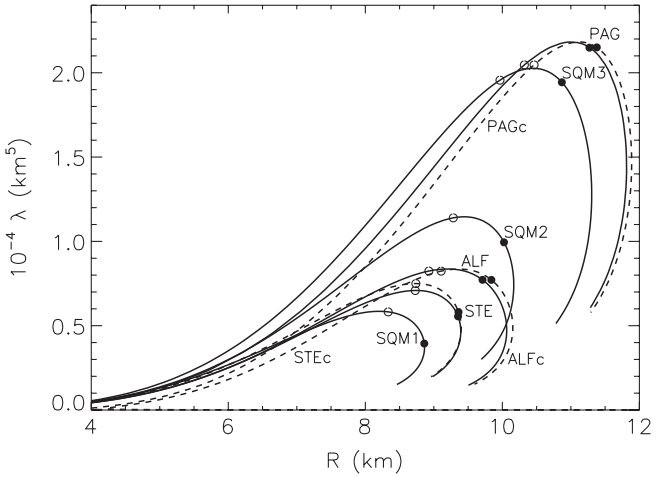

FIG. 14. Quadrupole polarizabilities λ for the strange quark matter stars. Filled (open) circles indicate configurations with $M = 1.4M_\odot$ $(1.0M_\odot)$. The solid and dashed curves are only intended for visual clarity.

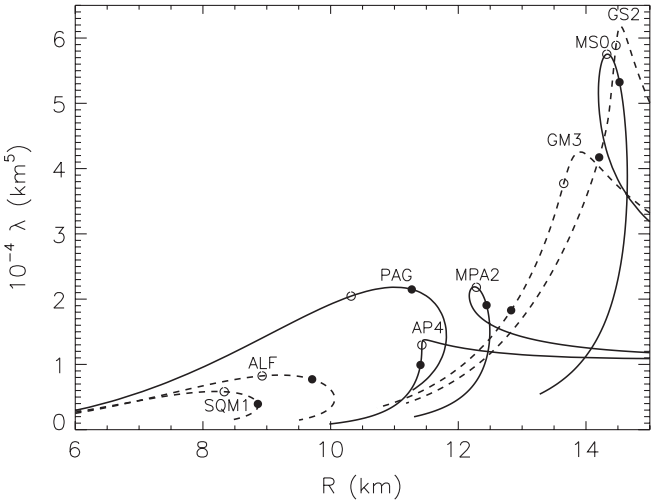

FIG. 15. Comparison of quadrupole polarizabilities λ for normal and strange quark matter stars. Filled (open) circles indicate configurations with $M = 1.4M_\odot$ $(1.0M_\odot)$. The solid and dashed curves are only intended for visual clarity.

solid crust produced by the tidal field is large enough, then the crust can be melted and our calculations become valid. The strength required to melt the crust can be estimated from the results of recent work on crust breaking. We estimate the induced quadrupole moment to be

$$Q_{22} = \lambda E_{22} \approx \lambda\sqrt{E_{ij}E^{ij}} = \sqrt{\frac{3}{2}}\lambda\frac{M}{D^3}, \tag{18}$$

where the tidal field strength E_{ij} [27] depends on the distance D between the stars and M is the total mass; we assumed for simplicity an equal-mass binary. Assuming a binary in circular orbit, we can calculate the orbital frequency Ω from Kepler's third law,

$$\Omega^2 \approx \frac{M}{D^3}. \tag{19}$$

Eliminating M/D^3 using Eq. (18), and recognizing that the frequency of the emitted gravitational waves f is twice the orbital frequency [28], we have

$$f = \frac{2}{2\pi}\Omega \approx \frac{1}{\pi}\sqrt{\frac{Q_{22}}{\lambda}}\left(\frac{2}{3}\right)^{1/4}, \tag{20}$$

which has an implicit mass dependence through Q_{22} and λ. For a $1M_\odot$ neutron star using the EOS labeled SLY, Horowitz [29] estimates that the maximum value of Q_{22} reached at the breaking point of the crust, where the strain $\sigma \approx 0.1$ [30], is approximately $Q_{22,\max} = 10^{40}$ g cm^2. The breaking point is therefore reached during the inspiral of an equal-mass binary at the moment when the frequency of detected gravitational waves becomes

$$f_{\rm br} \approx \frac{(2/3)^{1/4}}{\pi}\left(\frac{10^{40}\ {\rm g\,cm^2}}{2\times 10^{36}\ {\rm g\,cm^2\,s^2}}\right)^{1/2} \approx 20\ {\rm Hz}, \tag{21}$$

where we used the value for λ for a $1M_\odot$ star as determined in Fig. 9. Note that this frequency implies a binary separation distance $D_{\rm br} \approx 400$ km from Eq. (19). Therefore, when $D \le D_{\rm br}$ or $f \ge f_{\rm br}$, the shear from the induced quadrupole moment is strong enough to break the crust and beyond this point a solid crust can no longer exist. This frequency is below the observable region from 100 to 1000 Hz for current and proposed gravitational wave detectors such as LIGO [5]. Consequently, during the last stages of inspiral that are observed in gravitational waves, effects stemming from the solid crust are probably irrelevant and our calculations assuming a liquid phase should be valid.

Using the expressions provided by Owen [31], which are supported by our results, we can approximate the maximum quadrupole moment for a solid crust through

$$Q_{22,\max} = \frac{\sigma_{\max}}{0.01}\ {\rm g\,cm^2}\begin{cases} 2.4\times 10^{38}\left(\frac{R}{10\ {\rm km}}\right)^{6.26}\left(\frac{1.4M_\odot}{M}\right)^{1.2} & \text{neutron stars,} \\ 3.5\times 10^{39}\left(\frac{R}{8\ {\rm km}}\right)^{6}\left(\frac{1.4M_\odot}{M}\right) & \text{hybrid and meson-condensate stars,} \\ 2.8\times 10^{41}\frac{\mu}{4\times 10^{32}\ {\rm erg/cm^3}}\left(\frac{R}{10\ {\rm km}}\right)^{6}\left(\frac{1.4M_\odot}{M}\right) & \text{solid strange stars,} \end{cases} \tag{22}$$

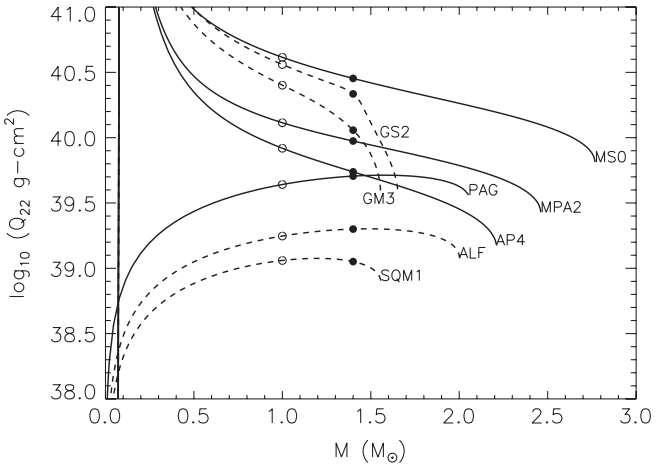

FIG. 16. The maximum quadrupole moment $Q_{22,\max}$ of a solid crust as a function of mass for normal and strange matter stars. Filled (open) circles indicate configurations with $M = 1.4M_\odot$ ($1.0M_\odot$). The solid and dashed curves are only intended for visual clarity.

where $\sigma_{\max} = 0.1$ is the breaking strain of the crust and $\mu \approx 4 \times 10^{32}$ erg/cm^3 is a typical shear modulus of a strange quark matter crust [30] which is a thousand times the typical value in the crust of a normal neutron star. The results are shown in Fig. 16. For stars with masses heavier than $1M_\odot$, the maximum quadrupole moments are within an order of magnitude of the typical value of 10^{40} g cm^2.

Figure 17 shows results for the breaking frequency $f_{\rm br}$ calculated utilizing Eq. (20) with the appropriate values for $Q_{22,\max}$ from Fig. 16. The breaking frequency for both kinds of stars heavier than a few tenths of a solar mass is well below the LIGO lower boundary of 100 Hz [5].

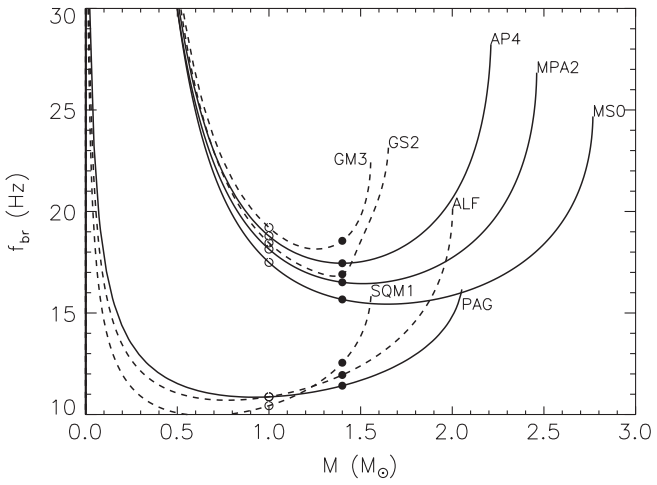

FIG. 17. The frequency of gravitational waves from an inspiraling binary when tidal forces are expected to break the crust for normal and strange quark matter stars. Filled (open) circles indicate configurations with $M = 1.4M_\odot$ ($1.0M_\odot$). The solid and dashed curves are only intended for visual clarity.

Therefore, the crust may be assumed to be melted during the time it is observed, and the approximation of treating the entire star as a liquid is justified.

VIII. SUMMARY AND CONCLUSIONS

The quadrupole polarizabilities of normal neutron stars and self-bound quark matter stars have been calculated for a wide class of proposed equations of state of dense matter for both normal and strange quark matter stars. The quadrupole polarizabilities $\lambda = 2R^5 k_2/(3G)$ are characterized by the dimensionless Love number k_2 and both are sensitive to the equation of state; in particular, to the compactness parameter M/R and the overall compressibility of the equation of state. For normal neutron stars, k_2 and λ exhibit pronounced maxima for configurations with masses close to a solar mass for most equations of state. The maximum value of k_2 is not very sensitive to the EOS, lying in the range 0.1–0.14. In each case, maximum mass configurations have significantly lower values of k_2 and λ than their solar mass counterparts.

Love numbers for self-bound strange quark matter stars with or without crusts are qualitatively different than those of normal neutron stars. The maxima in the values of k_2 for strange quark matter stars without crusts occur for masses less than $0.1M_\odot$, and maximum values of order 0.8 are achieved. As in the normal matter case, the maxima in quadrupole polarizabilities occur for configurations near $1M_\odot$. In contrast, the magnitudes of quadrupole polarizabilities of strange quark matter stars are usually much less than those of normal stars, owing to the larger radii of the latter.

Our investigations also point the need to examine the core-crust interface region of both normal and self-bound quark matter stars more closely than has been so far. The important issue that bears close scrutiny is the precise nature (first or second order) of possible phase transitions. In the case that strong discontinuities exist near the core-crust interface of strange quark matter stars, dimensionless Love numbers are suppressed for low mass stars relative to the cases for which there is no crust. However, for stars of order $1M_\odot$ or larger, the presence or absence of a crust has little influence on Love numbers.

The strength of the tidal signatures from coalescing compact binaries is proportional to λ, and is therefore quite sensitive to the radii of the stars. For stellar configurations with radii of order 11 km or less, the tidal response might be too small to observe, implying that a positive detection might be sufficient to rule out the presence of a self-bound star, such as a strange quark matter star, in the observed system.

The detectability of tidal signatures has been considered in some depth by Hinderer *et al.* [10]. For example, assuming a binary with equal $1M_\odot$ stars at a distance of 100 Mpc, they have estimated that Advanced LIGO could distinguish tidal love numbers $\lambda > \lambda_{\rm meas} \sim 6 \times 10^{36}$ g cm^2 s^2, which

in our units is equivalent to 4×10^{-4} km^5. In this case, only normal matter stars would have detectable tidal signatures. Stars with smaller masses or closer distances have smaller $\lambda_{\rm meas}$ ($\lambda_{\rm meas}$ scales as $DM^{2.5}$, where D is the distance and M is the mass), but there is no stellar evolutionary path for producing neutron or strange quark stars with smaller masses. Also, the event rate decreases with the cube of the distance, so it is unrealistic to appreciably decrease the reference distance. In the more likely case that the merging system contains 1.3–1.5$M_\odot$ stars, $\lambda_{\rm meas}$ exceeds 10^{-3} km^5 and Advanced LIGO would be unable to detect tidal signatures from any type of star. For the proposed Einstein telescope, Ref. [10] quotes a factor of 12 improvement in detectability, so that 1.4$M_\odot$ stars with radii greater than about 11 km might have detectable tidal signatures assuming $D = 100$ Mpc. Generally, strange quark stars have smaller radii and their tidal signatures would continue to remain undetectable.

It should also be noted that strange quark stars with the largest radii, which have masses and radii similar to those of normal neutron stars with relatively soft equations of state, have tidal Love numbers similar to those of normal stars. In the event that a binary containing at least one strange quark star was close enough and had a mass large enough to have a detectable tidal signature, our results imply that it would be extremely difficult to distinguish quark stars from normal neutron stars. This conclusion is similar to that reached by Hinderer *et al.* [10].

ACKNOWLEDGMENTS

The authors thank Ben Owen for alerting them to Love's importance. Thanks are also due to Dany Page, Andrew Steiner, and Mark Alford for providing equations of state based on their work. S. P. and M. P. acknowledge research support from the U.S. DOE Grant No. DE-FG02-93ER-40756. J. M. L. acknowledges research support from the U. S. DOE Grant No. DE-AC02-87ER40317.

APPENDIX A: BEHAVIOR OF y NEAR THE SURFACE FOR POLYTROPES

For polytropic equations of state with $n < 1$, the term $Q(r)$ defined in Eq. (4) diverges at the surface. To treat this divergence we first analyze the TOV equations, Eq. (9), in this case. With $p(\rho) = K\rho^{1+1/n}$, near the surface we have

$$K(1 + 1/n)\rho^{1/n}\frac{d\rho}{dr} \simeq -(\rho + K\rho^{1+1/n})\frac{M}{r(r-2M)}, \tag{A1}$$

where we have used the fact that $4\pi pr^3 \ll m \simeq M$. The solution is

$$\rho(r) \simeq \frac{1}{K^n}\left[\left(\frac{r(R-2M)}{R(r-2M)}\right)^{(1/(2(n+1)))} - 1\right]^n, \tag{A2}$$

using the boundary condition $\rho(R) = 0$. The squared adiabatic speed of sound is then

$$c_s^2 \simeq \frac{n+1}{n}\left[\left(\frac{r(R-2M)}{R(r-2M)}\right)^{(1/(2(n+1)))} - 1\right]. \tag{A3}$$

Now we change the radial variable to $s = R - r \ll R$ and expand the divergent term in $Q(r)$:

$$\frac{p+\rho}{c_s^2} \simeq \frac{n}{K^n(1+n)^n}\left[\frac{Ms}{R(R-2M)}\right]^{n-1}, \tag{A4}$$

where the divergence is evident from s^{n-1} when $n < 1$ and $s \to 0$. Assuming y to be finite at the surface, we keep only the divergent term in $Q(r)$ in Eq. (6); to lowest order in s, one finds

$$\frac{dy}{ds} \simeq 4\pi\frac{R^2}{R-2M}\frac{p+\rho}{c_{sn}^2}, \tag{A5}$$

where we have used $e^\lambda \simeq (1 - 2M/R)^{-1}$. This has the solution

$$y(s) = y_R + \frac{4\pi R^3}{M}\left[\frac{Ms}{K(1+n)R(R-2M)}\right]^n. \tag{A6}$$

The numerical integration for y is stopped near the surface at $s \ll R$, and y_R is computed from Eq. (A6).

APPENDIX B: PARAMETERS FOR ANALYTIC SOLUTIONS OF EINSTEIN'S EQUATIONS

We use the notation $\beta = GM/Rc^2$, $\alpha = 4\pi\rho_c R^2$, and $x = (r/R)^2$.

1. Uniform density ($\rho = \rho_c$)

$$\alpha = 3\beta, \qquad e^{-\lambda} = 1 - 2\beta x,$$
$$\frac{p}{\rho_c} = \frac{\sqrt{1-2\beta} - \sqrt{1-2\beta x}}{\sqrt{1-2\beta x} - 3\sqrt{1-2\beta}}, \tag{B1}$$
$$c_s^2 = \infty, \qquad \frac{\rho_s}{\rho_c} = 1.$$

2. Tolman VII ($\rho = \rho_c[1 - x]$) [15]

$$\alpha = \frac{15}{2}\beta, \quad e^{-\lambda} = 1 - \beta x(5 - 3x), \quad \frac{p}{\rho_c} = \frac{2}{15}\sqrt{\frac{3}{\beta e^\lambda}}\tan\phi - \frac{1}{3} + \frac{x}{5}, \quad \phi = \frac{w_1 - w}{2} + \phi_1, \quad \phi_1 = \tan^{-1}\sqrt{\frac{\beta}{3(1-2\beta)}},$$
$$w = \ln\left[x - \frac{5}{6} + \sqrt{\frac{e^{-\lambda}}{3\beta}}\right], \quad w_1 = \ln\left[\frac{1}{6} + \sqrt{\frac{1-2\beta}{3\beta}}\right], \quad c_s^2 = \frac{\tan\phi}{5}\left[\tan\phi + \sqrt{\frac{\beta}{3e^\lambda}}(5 - 6x)\right]. \tag{B2}$$

3. Buchdahl's solution ($\rho = 12\sqrt{p_* p} - 5p$) [20,21]

$$\alpha = \pi^2\beta(1-\beta)^2\frac{1-5\beta/2}{1-2\beta}, \qquad z = \frac{1-\beta}{1-\beta+u}\pi\sqrt{x}, \qquad u = \beta\frac{\sin z}{z}, \qquad e^{\lambda} = \frac{(1-2\beta)(1-\beta+u)}{(1-\beta-u)(1-\beta+\beta\cos z)^2},$$
$$c_s^2 = \frac{u}{1-\beta-4u}, \qquad \frac{\rho}{\rho_c} = \frac{(1-2\beta)(2-2\beta-3u)}{(2-5\beta)(1-\beta+u)^2}\frac{u}{\beta}, \qquad \frac{p}{\rho_c} = \frac{\beta(1-2\beta)}{(1-\beta+u)^2(2-5\beta)}\left(\frac{u}{\beta}\right)^2. \tag{B3}$$

4. Generalized Tolman IV ($N = 1$) [22,23]

$$\alpha = \frac{3\beta}{2}\frac{2-3\beta}{1-3\beta}, \qquad e^{\lambda} = \frac{1-3\beta+2\beta x}{(1-3\beta+\beta x)(1-\beta x)}, \qquad \frac{\rho}{\rho_c} = \frac{1-3\beta}{2-3\beta}\frac{(2-3\beta)(1-3\beta)+\beta(3-7\beta)x+2\beta^2x^2}{(1-3\beta+2\beta x)^2},$$
$$\frac{\rho_s}{\rho_c} = \frac{(1-2\beta)(1-3\beta)}{(1-3\beta/2)(1-\beta)}, \qquad \frac{p}{\rho_c} = \frac{1-3\beta}{2-3\beta}\beta\frac{1-x}{1-3\beta+2\beta x}, \qquad c_s^2 = \frac{1-3\beta+2\beta x}{5-15\beta+2\beta x}. \tag{B4}$$

5. Generalized Tolman IV ($N = 2$) [22,23]

$$\alpha = 3\beta\left(\frac{2-2\beta}{2-5\beta}\right)^{2/3}, \qquad e^{-\lambda} = 1-2\left(\frac{2-2\beta}{2-5\beta+3\beta x}\right)^{2/3}\beta x, \qquad \frac{\rho}{\rho_c} = \left(1+\frac{5\beta x}{3(2-5\beta)}\right)\left(1+\frac{3\beta x}{2-5\beta}\right)^{-5/3},$$
$$\frac{\rho_s}{\rho_c} = \frac{(1-5\beta/3)(1-5\beta/2)^{2/3}}{(1-\beta)^{5/3}}, \qquad \frac{p}{\rho_c} = \left(\frac{2-5\beta}{2-2\beta}\right)^{2/3}\frac{1}{3(2-5\beta+\beta x)}\left[2-\left(\frac{2-2\beta}{2-5\beta+3\beta x}\right)^{2/3}(2-5\beta+5\beta x)\right],$$
$$c_s^2 = \frac{2-5\beta+3\beta x}{5(2-5\beta+\beta x)^3}\left[\frac{(2-5\beta+3\beta x)^{5/3}}{(2-2\beta)^{2/3}}+(2-5\beta)^2-5\beta^2x^2\right]. \tag{B5}$$

[1] C. Cutler *et al.*, Phys. Rev. Lett. **70**, 2984 (1993).
[2] B. P. Abbott *et al.* (LIGO Scientific), Phys. Rev. D **79**, 122001 (2009).
[3] C. S. Kochanek, Astrophys. J. **398**, 234 (1992).
[4] C. Cutler and E. E. Flanagan, Phys. Rev. D **49**, 2658 (1994).
[5] B. Abbott *et al.*, Phys. Rev. D **69**, 122001 (2004).
[6] J. M. Lattimer and M. Prakash, Astrophys. J. **550**, 426 (2001).
[7] L. Bildsten and C. Cutler, Astrophys. J. **400**, 175 (1992).
[8] E. E. Flanagan and T. Hinderer, Phys. Rev. D **77**, 021502 (2008).
[9] A. E. H. Love, Proc. R. Soc. A **82**, 73 (1909).
[10] T. Hinderer, B. D. Lackey, R. N. Lang, and J. S. Read, arXiv:astro-ph/09113535.
[11] T. Damour and A. Nagar, arXiv:gr-qc/09061769.
[12] J. M. Lattimer and B. F. Schutz, Astrophys. J. **629**, 979 (2005).
[13] K. Thorne and A. Campolattaro, Astrophys. J. **149**, 591 (1967).
[14] T. Hinderer, Astrophys. J. **677**, 1216 (2008).
[15] R. C. Tolman, Phys. Rev. **55**, 364 (1939).
[16] J. R. Oppenheimer and G. M. Volkoff, Phys. Rev. **55**, 374 (1939).
[17] R. A. Brooker and T. W. Olle, Mon. Not. R. Astron. Soc. **115**, 101 (1955).
[18] K. D. Kokkotas and G. Schäfer, Mon. Not. R. Astron. Soc. **275**, 301 (1995).
[19] T. Binnington and E. Poisson, Phys. Rev. D **80**, 084018 (2009).
[20] H. A. Buchdahl, Phys. Rev. **116**, 1027 (1959).
[21] H. A. Buchdahl, Astrophys. J. **146**, 275 (1966).
[22] H. Nariai, Sci. Rep. Tohoku Univ. Ser. 1 **34**, 160 (1950).
[23] K. Lake, Phys. Rev. D **67**, 104015 (2003).
[24] P. Jaikumar, S. Reddy, and A. W. Steiner, Phys. Rev. Lett. **96**, 041101 (2006).
[25] D. P. Page (private communication).
[26] M. G. Alford (private communication).
[27] M. Favata, Phys. Rev. D **73**, 104005 (2006).
[28] L. D. Landau and E. M. Lifshitz, *The Classical Theory of Fields* (Pergamon Press, London, 1975), 2nd ed.
[29] C. J. Horowitz, Phys. Rev. D **81**, 103001 (2010).
[30] C. J. Horowitz and K. Kadau, Phys. Rev. Lett. **102**, 191102 (2009).
[31] B. J. Owen, Phys. Rev. Lett. **95**, 211101 (2005).
[32] J. M. Lattimer and M. Prakash, Astrophys. J. **550**, 426 (2001).
[33] M. Prakash, J. R. Cooke, and J. M. Lattimer, Phys. Rev. D **52**, 661 (1995).
[34] F. Douchin and P. Haensel, Astron. Astrophys. **380**, 151 (2001).
[35] P. Haensel, S. BonazzolaM. Salgado, and M. Salgado, Astron. Astrophys. **296**, 745 (1995).
[36] G. Baym, C. Pethick, and P. Sutherland, Astrophys. J. **170**, 299 (1971).